INT. J. NUM. METH. HEAT FLUID FLOW, VOL. 2, 37–53 (1992)

A STUDY OF MIXED GEOMETRICAL AND ROTATIONAL EFFECTS ON INTERNAL TURBULENT FLOW AND HEAT TRANSFER

C. TAYLOR and J. Y. XIA

Departments of Civil Engineering, and Materials Engineering, University College of Swansea, Swansea SA2 8PP, UK

ABSTRACT

A finite element method based investigation is carried out for the determination of three-dimensional turbulent flow structures and heat transfer rates of cooling ducts within turbine blades which rotate about an axis orthogonal to their own axis of symmetry. The effects of geometrical configurations, Coriolis forces and coolant inertias on the hydrodynamic and thermal characteristics have been systematically predicted and compared with experimental measurements.

KEY WORDS Internal turbulent flow Cooling ducts Finite element modelling

INTRODUCTION

For over a decade the quest for improved aero gas turbine power and fuel economy has stimulated much research interest in the design of high performance cooling systems for rotor blade airfoil sections. Current state of the art cooling systems require complex air flow passages to be incorporated inside the rotating airfoil section. These passages, channelling compressor-bled air in a spanwise direction along the blade, may have a variety of smooth or artificially roughened cross-sectional shapes with interconnecting bends if the coolant flows in a multi-pass manner.

In general terms, a fluid flowing through such cooling passages, which are rotating about an axis orthogonal to their longitudinal axis, is subjected to additional inertial effects known as Coriolis and centripetal accelerations. The centripetal acceleration components are dependent on the location of a fluid particle with respect to the axis of rotation of the duct and are conservative in nature. The Coriolis acceleration is dependent on the vector product of the rotational vector describing the duct rotation and the relative velocity field itself. This product generates a strong secondary flow in planes perpendicular to the main spanwise flow direction. The resulting spiralling flow along the duct causes core region fluid to move towards the trailing or rearward edge of the duct with a return flow along the duct periphery towards the leading or forward edge.

Obviously, several factors can affect the hydrodynamic characteristics of this strong secondary flow and, consequently, the thermal cooling efficiency of these air flow passages. The first factor is the geometrical configuration. Since the secondary flows are formed mainly due to the bounded surfaces, different shapes of cross-sections will produce different patterns of the transverse flow. If ribs or fins are located along the internal surface of the ducts, this flow mechanism is further complicated with the interaction of longitudinal separation flows in the vicinity of ribs. The second factor is the relative rotational magnitude, named Rossby number, which reflects the ratio between the Coriolis force and the flow inertia. A higher Rossby number implies a stronger transverse flow, hence a larger circumferential variation of heat transfer rates.

The combination of these factors are so complicated that the experimental observations[1,2]

0961–5539/92/010037–17$2.00

Received September 1991

usually only provide a bulk variation of heat transfer in an average sense although a recent contribution[3] indicates that detailed observations are now possible. Therefore, the main aim of this paper, based on the finite element modelling technique, is to simulate the detailed process of turbulent flow and heat transfer under the mixed geometric, rotational and inertial effects within turbine blade cooling ducts.

GOVERNING EQUATIONS AND FINITE ELEMENT FORMULATION

The current investigation relates to steady-state, incompressible turbulent flows through coolant passages within aircraft turbine blades which rotate about an axis orthogonal to its longitudinal axis. For such a situation, the governing equations, the modified Navier–Stokes equations including coriolis and centripetal effects, are,

$$\rho U_j \frac{U_i}{\partial x_j} = -\frac{\partial P}{\partial x_i} + \frac{\partial}{\partial x_j}\left[(\mu+\mu_t)\left(\frac{\partial U_i}{\partial x_j}+\frac{\partial U_j}{\partial x_i}\right)\right]+X \tag{1}$$

in which repeated suffices are used, x_i denotes an orthogonal coordinate direction, U_i the corresponding velocity, ρ the fluid density, P the local pressure, μ and μ_t the dynamic and turbulent viscosity, respectively, and X a body force defined by:

$$X = 2\rho(\bar{\Omega}\times\bar{U})\cdot\bar{I}+\rho\Omega_j^2 x_i \sin(\Omega_j x_i) \tag{2}$$

where $\bar{\Omega}$ is a rotational vector, $\bar{U}$ the fluid velocity vector, $\bar{I}$ a unit vector and (Ω_j, x_j) are angles between the rotating and unit vectors.

The centripetal terms in (2) are conservative and may be absorbed into the pressure gradient term if the fluid is assumed to have invariant properties.

The flow field must satisfy the conservation of mass which, in the present context, may be written as,

$$\frac{\partial U_i}{\partial x_i}=0 \tag{3}$$

Equations (1)–(3) cannot be solved unless a turbulence closure model is provided to evaluate the turbulent contribution to the effective viscosity $\mu_e=\mu+\mu_t$. For the present work, a (K–l) one-equation model has been adopted so that,

$$\mu_t = C_\mu \rho K^{1/2} l \tag{4}$$

where C_μ is a constant, K the turbulence kinetic energy, $l=l_m$ and the length scale 'l_m' is based on the Prandtl mixing length, which is taken for present purposes, as 0.4 times the normal distance from the nearest wall surface. The distribution of turbulent kinetic energy (K) is depicted by the transport equation.

$$\rho U_i \frac{\partial K}{\partial x_i} = \frac{\partial}{\partial x_j}\left[\left(\mu+\frac{\mu_t}{\sigma_k}\right)\frac{\partial K}{\partial x_j}\right]+\mu_e\frac{\partial U_i}{\partial x_j}\left(\frac{\partial U_j}{\partial x^i}+\frac{\partial U_i}{\partial x_j}\right)-C_D\rho K^{3/2}/l \tag{5}$$

in which σ_k is the turbulence Prandtl type number and C_D is a constant.

An inherent problem when analysing confined turbulent flows and using a numerical approach is mapping within the conventionally termed 'near wall zone'. In order to accommodate the rapid transfer of shear and variations in both velocities and turbulent kinetic energy, the region would, if conventional techniques are employed, require an extremely fine spatial subdivision. A commonly used approach is, therefore, to terminate the actual computational domain at a small distance from the solid surface. The above governing equations are then solved, using a numerical method, everywhere within this domain. The conditions specified at the edge of the resulting near wall zone are subject to simultaneous correspondence between the main flow domain and the near wall zone. In the near wall zone the variation in velocity can be evaluated using either the conventional logarithmic function representation or a unidimensional modelling[4]. The convective heat transfer associated with such confined turbulent

flows, however, is not straightforward, since, (i) no empirical functions exist at the edge of the near wall zone to provide boundary conditions for heat transfer, and (ii) the source of heat is usually known either on the outer extremity or within the confining solid.

In order to obtain an accurate simulation of heat transfer from the outer face of the solid into the flow, corresponding to experimental conditions[5], the solid must be included in the discretized form of the finite element procedure. The energy conservation, for the fluid, is expressed as,

$$\rho C U_j \frac{\partial T}{\partial x_j} = \frac{\partial}{\partial x_i}\left[C\left(\frac{\mu}{\sigma} + \frac{\mu_t}{\sigma_t}\right)\frac{\partial T}{\partial x_i}\right] \tag{6}$$

and within the containing solid, since no convention terms exist,

$$\frac{\partial}{\partial x_j}\left(k\frac{\partial T}{\partial x_i}\right) = 0 \tag{7}$$

Along the interface between the solid and fluid, the continuity of heat transfer is automatically satisfied since the finite element method assumes the continuity of flux along the internal element boundaries, i.e.

$$\int_{\text{fluid}} C\left(\frac{\mu}{\sigma} + \frac{\mu_t}{\sigma_t}\right)\frac{\partial T}{\partial n}\mathrm{d}S = \int_{\text{solid}} k\frac{\partial T}{\partial n}\mathrm{d}S \tag{8}$$

where n is the normal unit outward vector at the interface, C the specific heat at constant pressure of the fluid, k the thermal conductivity of the solid. σ_t is a turbulent temperature Prandtl type number.

All constant values used in the above equations (1)-(8) are as in Reference 6,

$$\sigma = 0.7, \quad \sigma_k = 0.645, \quad C_D = 0.4184, \quad C_\mu = 0.22, \quad k = 1.293$$

$$\sigma_t = \begin{cases} 0.7 & y^+ \leqslant 5 \\ 1.4 - \dfrac{0.7(13 - y^+)}{8} & 5 < y^+ \leqslant 13 \\ 1.4 & 13 < y^+ \leqslant 17 \\ 0.95 + \dfrac{0.45(25 - y^+)}{8} & 17 < y^+ \leqslant 25 \\ 0.95 & y^+ > 25 \end{cases}$$

where $y^+ = \dfrac{y}{v}\sqrt{\dfrac{\tau_0}{\rho}}$

y = normal distance from the wall

τ_0 = wall shear stress

$v = \dfrac{\mu}{\rho}$

PROBLEM DESCRIPTION AND BOUNDARY CONDITIONS

To demonstrate the theoretical methods being developed and the supportive role of fundamental experimentation with which to attempt validation and improvement of those theoretical methods, cylindrical ducts, as in *Figure 1*, with either smooth internal wall surface or five transverse ribs equally spaced in the axial direction as shown in *Figure 2*, have been taken as the computational domain. The duct length L is 130 mm, the inner diameter D is 10 mm and the mid-span eccentricity H is 335 mm. For the ribbed duct, the ratio of rib height to inner duct diameter (h/D) is 0.2 and the ratio of rib height to pitch (h/l_p) is 0.1. *Figure 3* shows the finite element mesh used for the prediction of the primitive variable (a) and heat transfer (b). The mesh used to evaluate heat

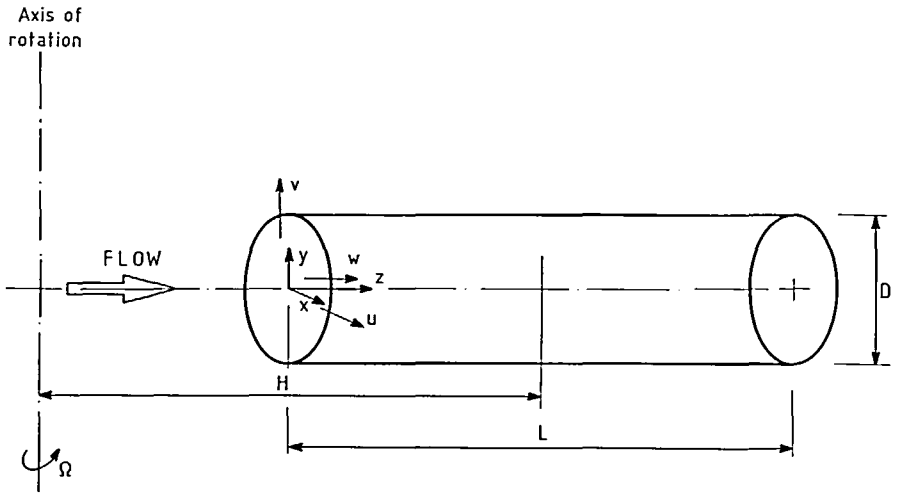

Figure 1 Geometry and coordinate system

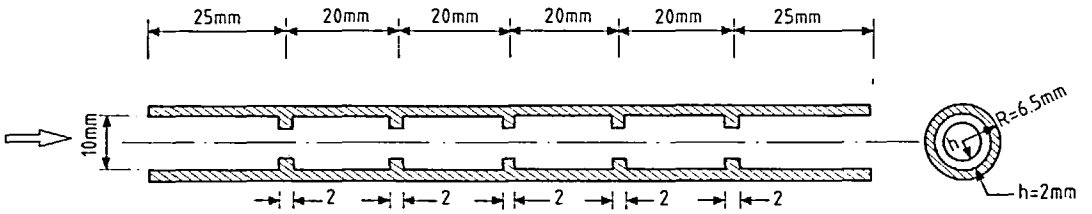

Figure 2 Geometry of the ribbed duct

transfer is evolved from that used to predict the flow by adding extra elements to include the near wall zone and the solid region.

The upstream boundary conditions relating to velocity correspond to a zero transverse flow and an axial velocity profile based on the 1/7 power law corresponding to a Reynolds number. The kinetic energy proile is taken as 1% of the squared mean axial velocity component. Updated traction boundary conditions[7] are applied at the downstream boundary. In the near wall zone, a logarithmic universal law[8] is used to depict the variation in the velocity.

For heat transfer system, based on the present coupled solid/fluid approach, the specified boundary conditions are as shown on *Figure 4*. At inlet, measured temperatures for the solid wall, T_{w0}, and fluid, T_{f0}, are specified; along the outer wall surface, an experimentally determined heat flux is applied. These known conditions are taken from a report[9] prepared by Rolls-Royce plc. At exit, since flux conditions inside the flow domain are unknown, arbitrary heat flux values,

$$f_i = \left(\frac{\mu}{\sigma} + \frac{\mu_t}{\sigma_t}\right)\frac{\partial T}{\partial n} \tag{9}$$

in which n is the component of a unit outward normal to the boundary, imposed as an initial condition and subsequently updated to be compatible with the heat flux from within the flow domain. This results in a necessarily iterative solution procedure. Around the exit solid surface, either temperature or heat flux profiles, if available, can be specified. A detailed solution procedure can be found in Reference 6.

The coupled solid/fluid model for heat transfer in a complex geometry comprising the

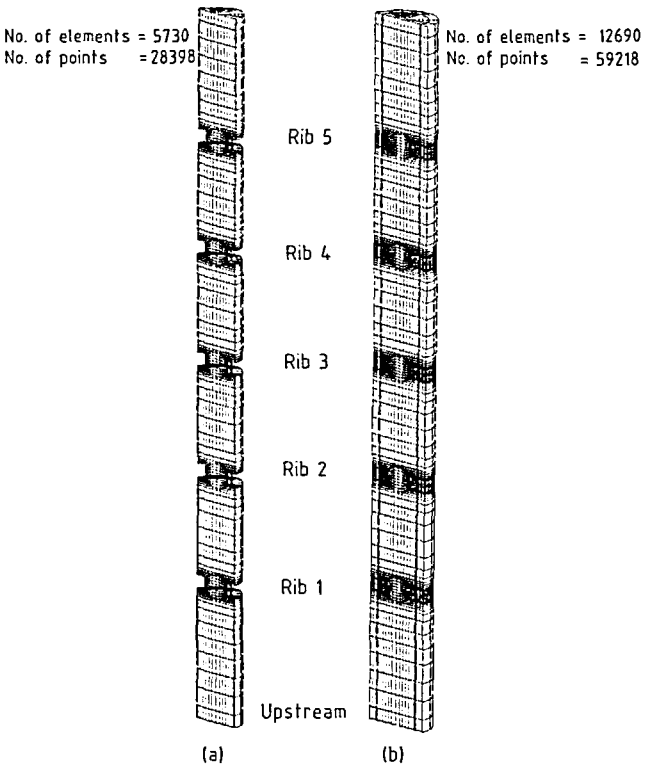

Figure 3 Finite element mesh used: (a) for evaluation of flow; (b) for evaluation of heat transfer

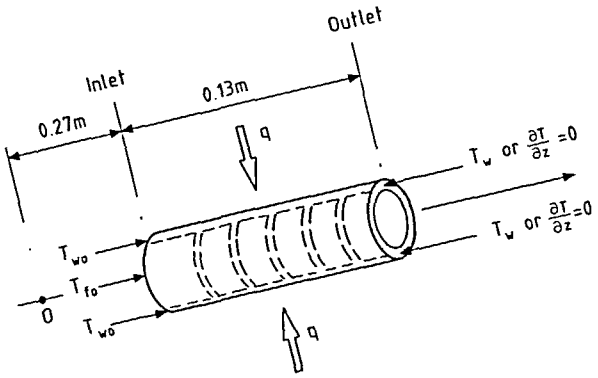

Figure 4 Specified boundary conditions for heat transfer

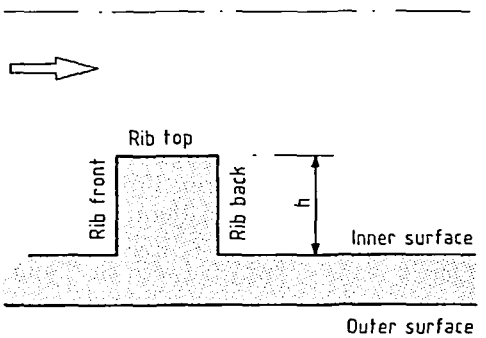

Figure 5 Definition of some terms relating to ribs

multi-ribbed duct is extremely effective since the distribution of heat flux around each ribbed surface from rib front to rib back (*Figure 5*) varies rapidly and is automatically evaluated in the numerical model and would be extremely difficult to measure.

PRESENTATION AND DISCUSSION OF RESULTS

The validation of the above detailed computational model has been presented in the previous papers[10,11], in which the direct comparisons of profiles for both turbulent flow and heat transfer

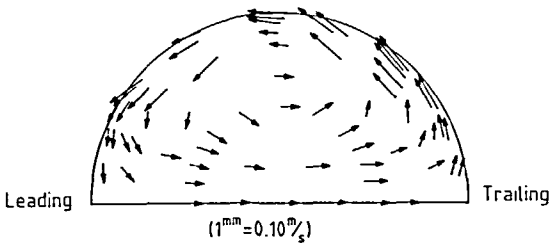

Figure 6 Secondary velocity patterns of fully developed turbulent flows in a rotating pipe (Re = 15,000; Ω = 2700 rev/min)

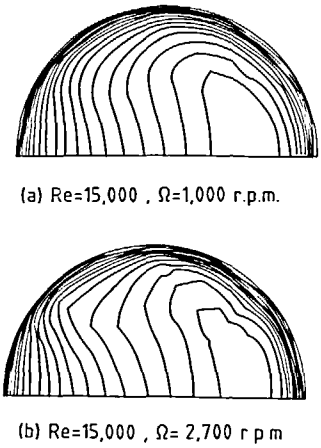

Figure 7 Effects of Coriolis forces on the axial velocity contours for fully developed turbulent flows in a rotating pipe

between the numerical prediction and the experimental measurements have been made and the importance of the inclusion of the wall conduction has been demonstrated. In this paper, attention is focused on the geometrical, rotational and inertial effects on both the hydrodynamic and thermal characteristics within the coolant ducts.

The effect of Coriolis forces on the flow profiles within the smooth rotating pipe are indicated in *Figure 6* for the secondary motion and *Figure 7* for the axial velocity components. Due to rotation, a Coriolis force is imposed on each particle, which results in a particle with a high velocity, occurring in central region, moving faster than those around the near wall region and hence is forced to move by the incoming fluid towards the rotating trailing edge. As a consequence, a secondary flow pattern is generated and the peak of the axial velocity profile is shifted towards the trailing edge. The higher the rotational speed, the larger the shift, as shown on *Figure 7.*

When this computational model is applied to a rotating multi-ribbed cylindrical duct, the situation becomes much more complicated. *Figures 8* and *9* are plots of the axial velocity profiles along the symmetric plane for the Reynolds number $Re = 15{,}000$ and three different values of Rossby number 0.04, 0.08 and 0.12. The influence of rotation on the entry region, say from inlet up to the first rib, is negligible and the first rib geometry is the dominant factor influencing the flow pattern over the rib. From the downstream of the first rib, both the rib geometry and rotation affect the flow pattern. Unlike the smooth duct, the effects of rotation vary with locations in the ribbed duct. *Figure 10* shows the contour plots of axial velocity for two different locations. One is at the midway between rib 3 and rib 4, the other is at the top of rib 4. With increasing Rossby number the change in pattern and the progress of the maximum velocity towards the trailing edge is much more apparent over the ribs than at the mid section. This is to be expected since the Coriolis force is the vector product of the duct rotation vector and the relative flow field.

A further comparison of the axial flow field is made by plotting the profiles of both the longitudinal velocity component and the kinetic energy for different rotational speeds. This is shown on *Figure 11* where the plots are along the line of symmetry between the leading edge and the trailing edge at a section midway between each pair of ribs. For the stationary duct, since no Coriolis force induced secondary flow is produced, the longitudinal flow is axisymmetric so that the magnitude and the width of the recirculation zone is circumferentially uniform. When rotation is introduced, the flow pattern is restructured by the appearance of secondary flow. With increasing rotational speed the magnitude and width of the recirculation zone increases at the leading edge and decreases at the trailing edge (see *Figure 9*).

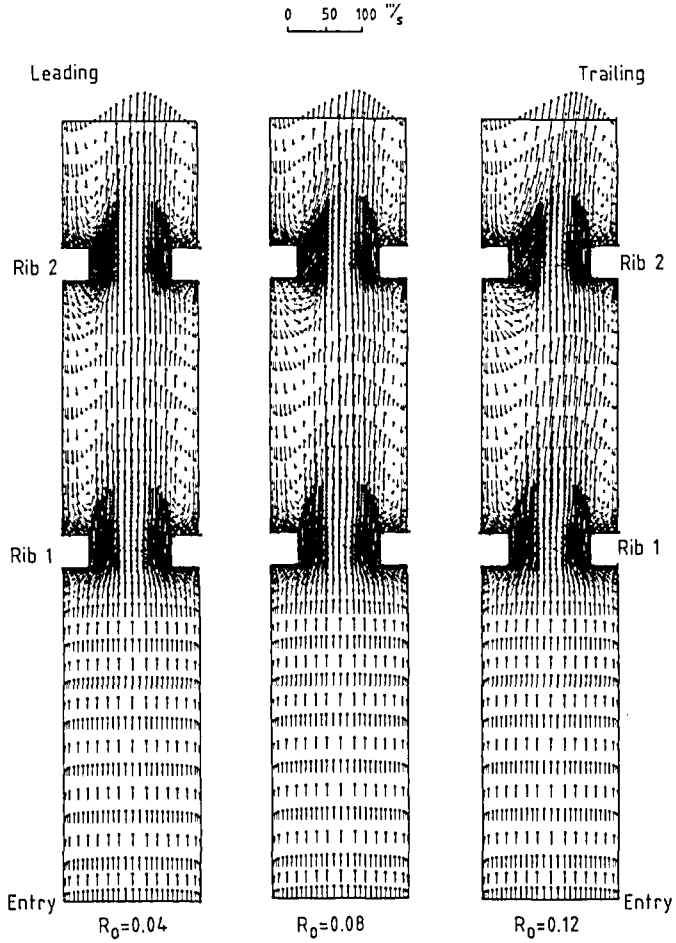

Figure 8 Predicted effects of Rossby number on the axial velocity profiles along the symmetric plane in a ribbed cylindrical duct (Re = 15,000)

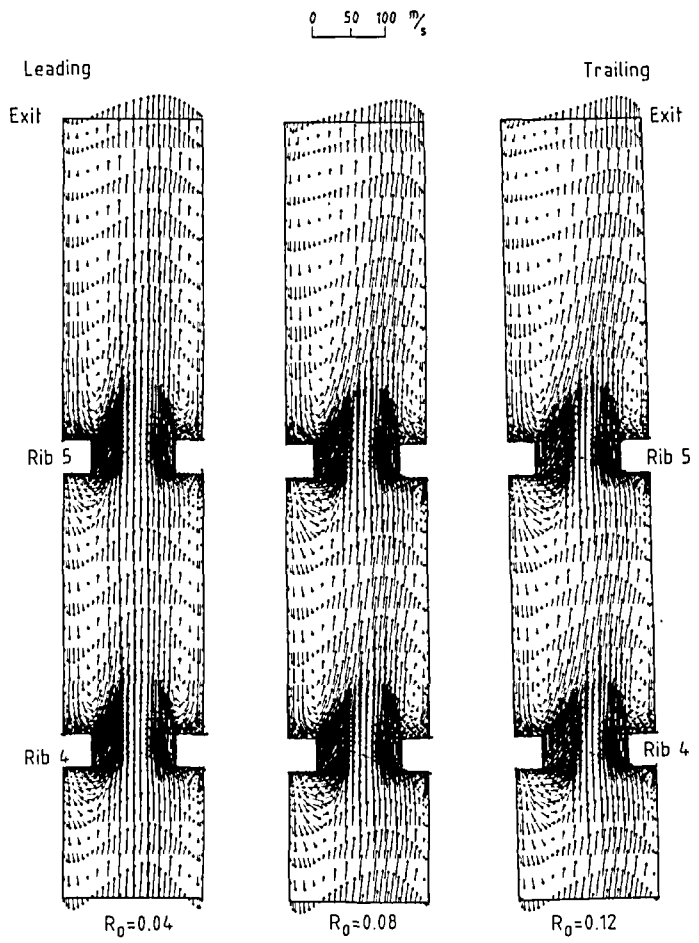

Figure 9 Predicted effects of Rossby number on the axial velocity profiles along the symmetric plane in a ribbed cylindrical duct (Re = 15,000)

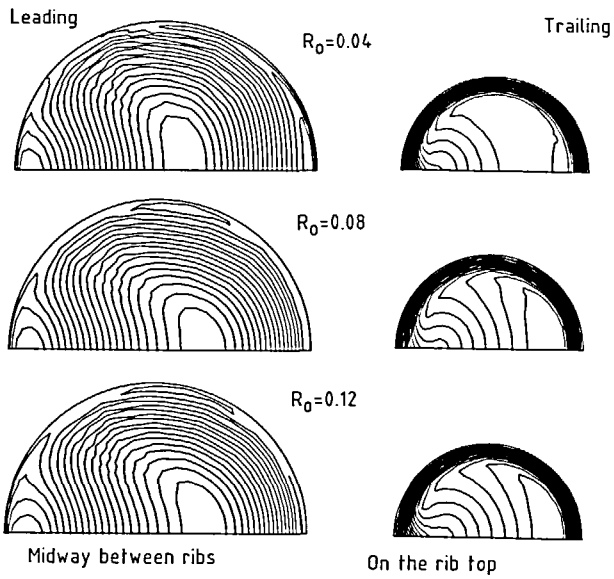

Figure 10 Predicted effects of Rossby number on the pattern of axial velocity contour in a ribbed cylindrical duct (Re = 15,000)

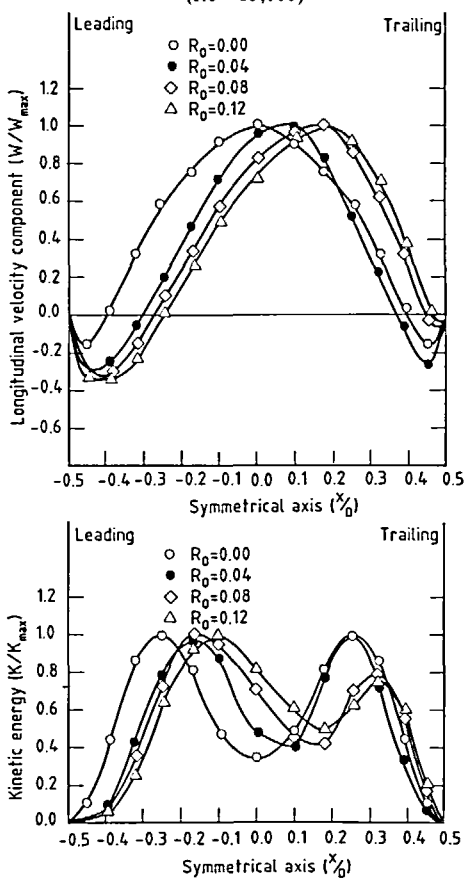

Figure 11 Predicted effects of Rossby number on the axial velocity (W) and kinetic energy (K) profiles in a ribbed cylindrical duct (Re = 15,000)

The development of the secondary flow when ribs are present is far more complicated than that in a smooth duct. *Figures 12* and *13* show the influence of Rossby number on the repeating secondary flow patterns as well as the variation at specific axial locations. On the rib top, the overall pattern of the secondary recirculation is little affected with increasing Rossby number. This is also true at the location immediately after a rib exit. However, midway between ribs, the imposition of the Coriolis force becomes more pronounced and the pattern changes significantly with increasing Rossby number. At a Rossby number of $Ro=0.04$, the recirculation zones at

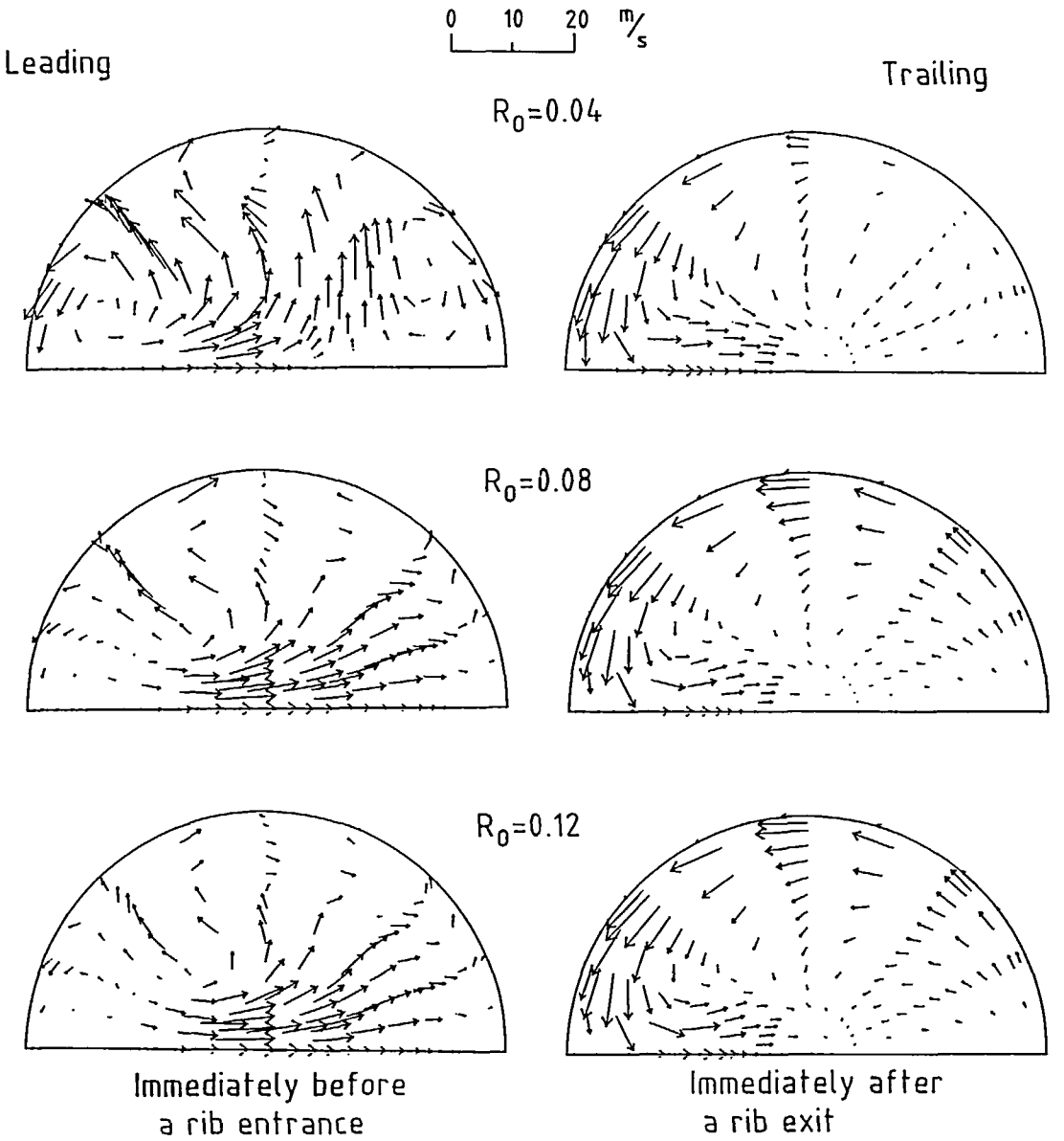

Figure 12 Predicted effects of Rossby number on the pattern of secondary velocity vectors in a ribbed cylindrical duct (Re = 15,000)

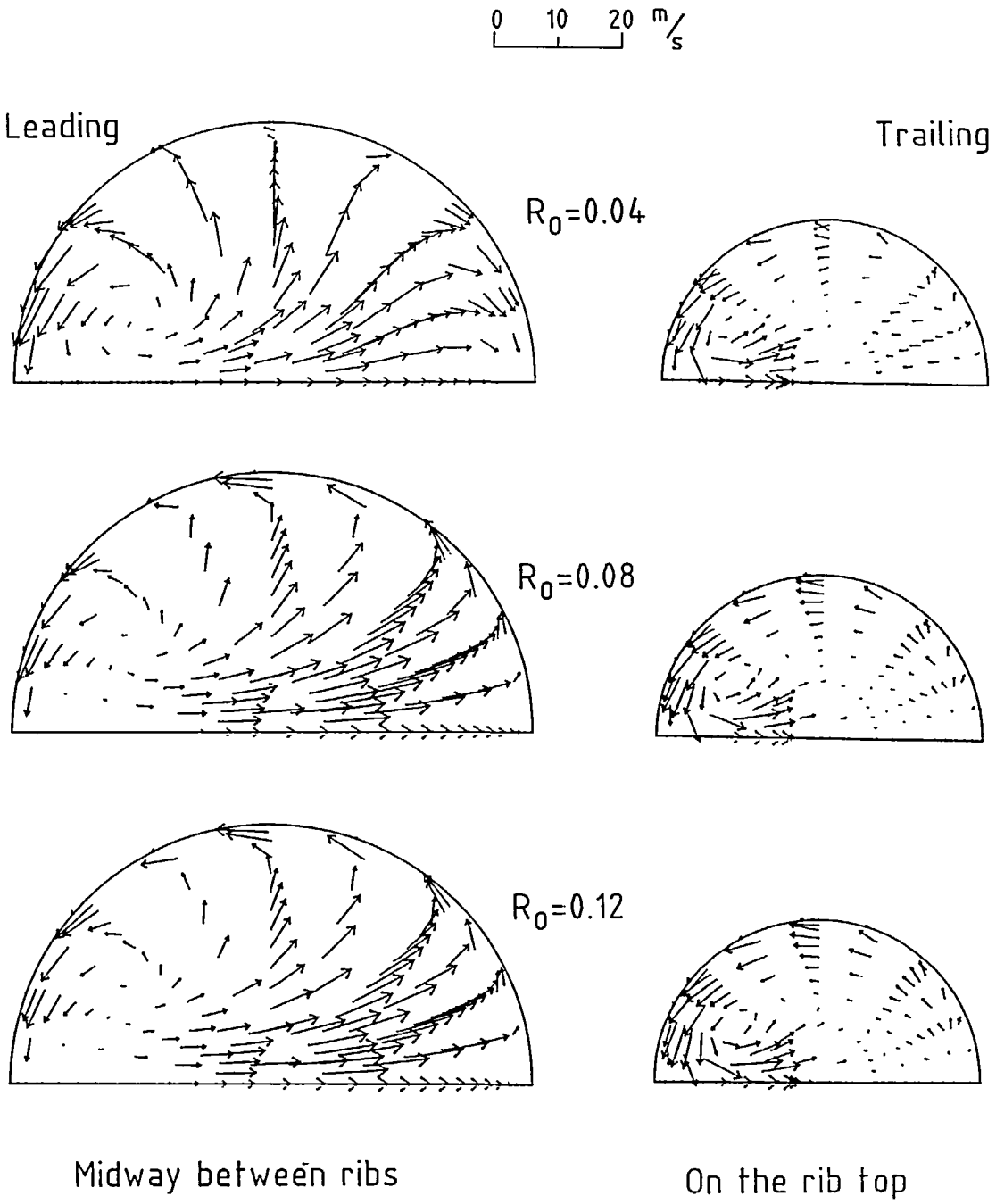

Figure 13 Predicted effects of Rossby number on the pattern of secondary velocity vectors in a ribbed cylindrical duct (Re = 15,000)

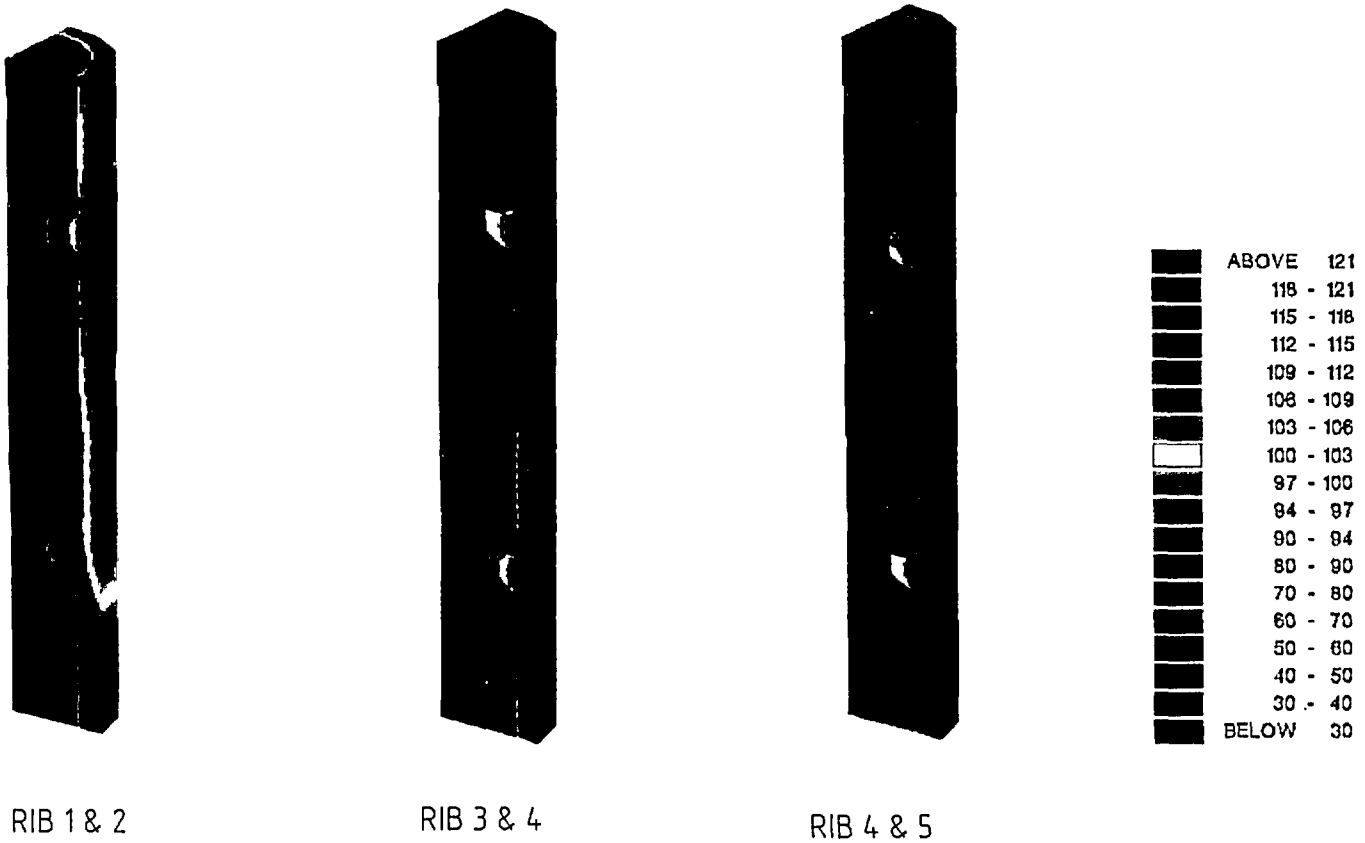

Figure 14 Temperature contour (°C) for a stationary ribbed duct ($Re = 15{,}000$)

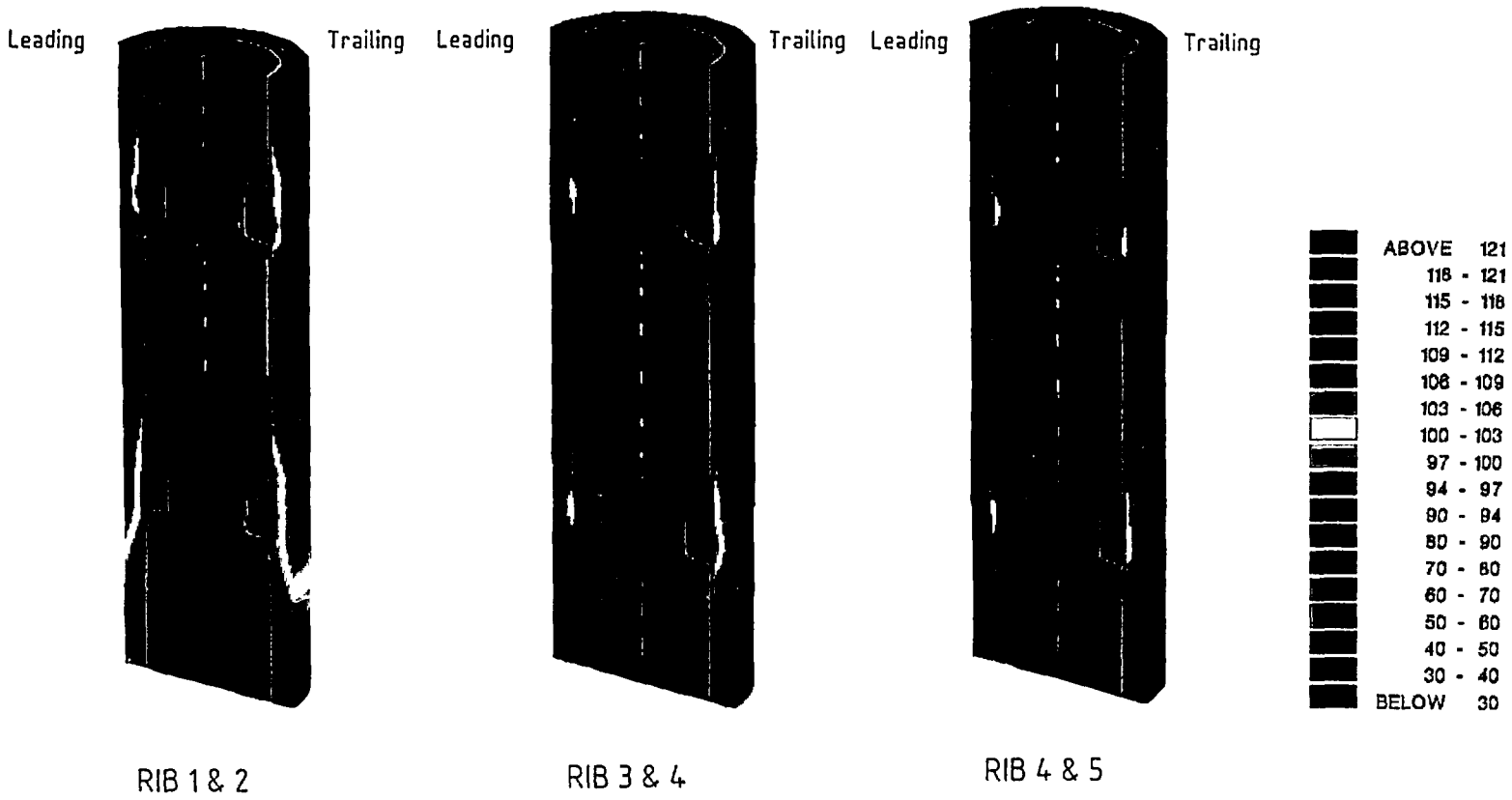

Figure 15 Temperature contour (°C) for a rotating ribbed duct ($Re = 15{,}000$, $Ro = 0.04$)

both the leading and trailing edge affects transfer of momentum between the longitudinal and transverse directions when the Rossby number is increased to 0.08, this transfer process reduces at the trailing edge but is enhanced at the leading edge. This phenomenon becomes more obvious with a further increase in Rossby number to 0.12.

The consequence of this complex flow structure results in a complicated thermal profile. *Figures 14* and *15* show the temperature contours, degree centrigrade, within the solid wall as well as the flow domain, corresponding to the stationary and rotating ribbed ducts respectively. For the stationary ribbed duct, only a quarter of the cylinder is plotted. The hotter zones are within the solid at the ribs corresponding to the location of low circulation. Within the fluid, the temperature steadily increases in a downstream direction as heat is transferred from the solid into the fluid. When the duct is rotating, the contours are distorted towards the trailing edge, which is expected, so that the heat flow to the fluid at the trailing edge is larger than that at the leading edge. Comparing corresponding contours for the stationary duct, the most significant change is the location of hotter regions. These now occur at the midway between the ribs as opposed to adjacent to the ribs.

The enhancement of heat transfer due to the incorporation of ribs is apparent, as shown in *Figure 16*, and is enhanced by up to 100% compared with that in a smooth duct. The influence of rotation is generally quantified in terms of Rossby number, *Ro*. For Rossby number 0.04, as in *Figure 16*, the effect of rotation on heat transfer in a ribbed duct is only local and there is no discernible overall increase with longitudinal distance downstream. However, as the Rossby number increases, a certain amount of overall increase of heat transfer is predicted, as shown in *Figures 17* and *18*. At Rossby numbers from 0.04 and 0.08 there is no significant variation in heat transfer particularly close to the ribs. This indicates that for the range of parameters studied, inclusion of the ribs is the dominant fact. For values of Rossby numbers greater than 0.08, the Coriolis effect increases (*Figure 17*) for the trailing edge. In contrast to *Figure 17*, *Figure 18* for the leading edge shows a relatively small variation and is limited to the regions away from the ribs.

The flow capacity, in terms of Reynolds number, reflects the carrying capacity of heat from the surrounding wall surface. *Figures 19*, *20* and *21* show, quantitatively, the heat transfer profiles for two sets of Reynolds number, 15,000 and 30,000 at different rotational speeds. These Figures

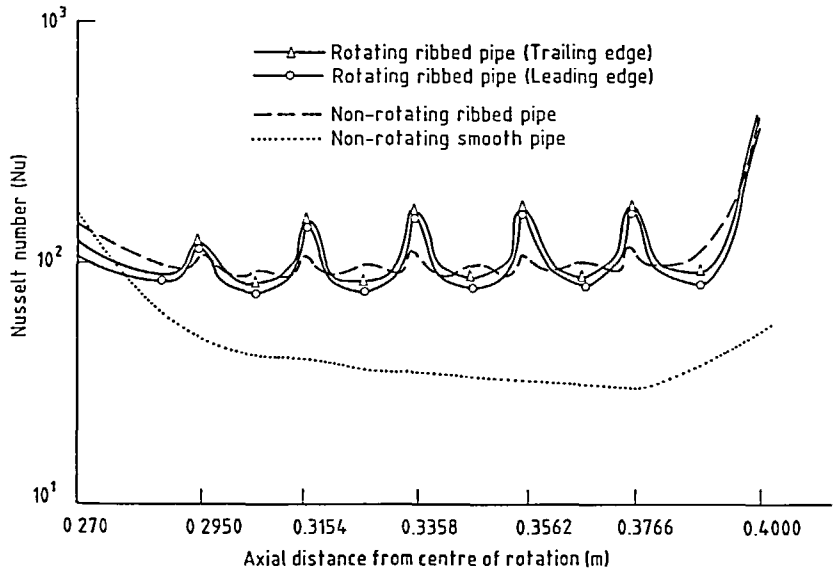

Figure 16 Comparison of heat transfer (*Nu*) along the *inner surface* of cooling duct (Re = 15,000; Ω = 1000 rev/min)

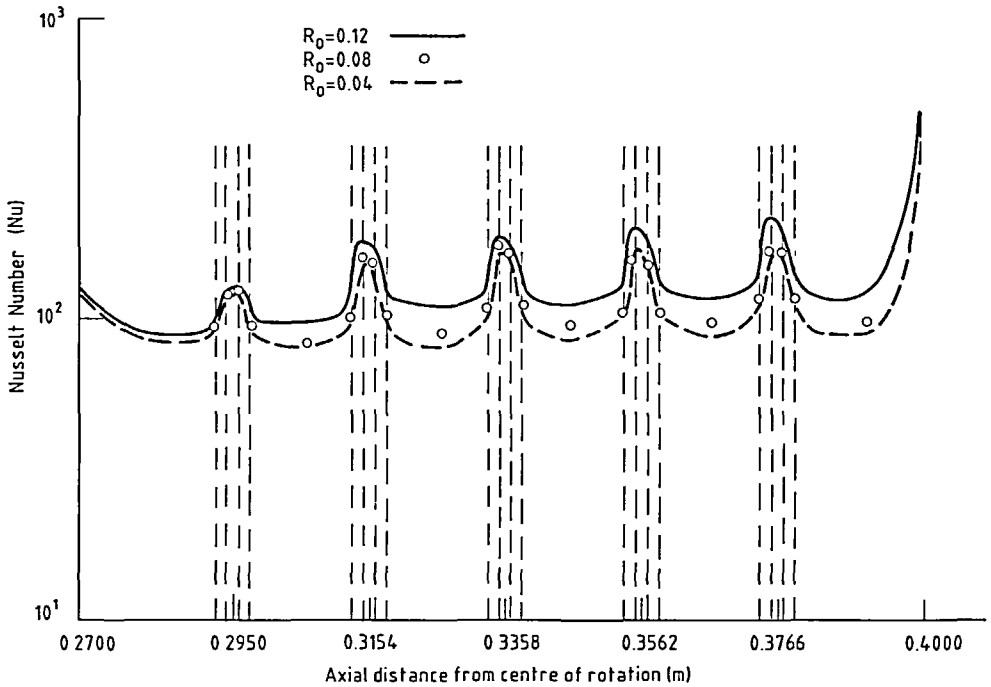

Figure 17 Predicted effects of Rossby number on the heat transfer (*Nu*) along the trailing edge of a ribbed cylindrical duct (Re = 15,000)

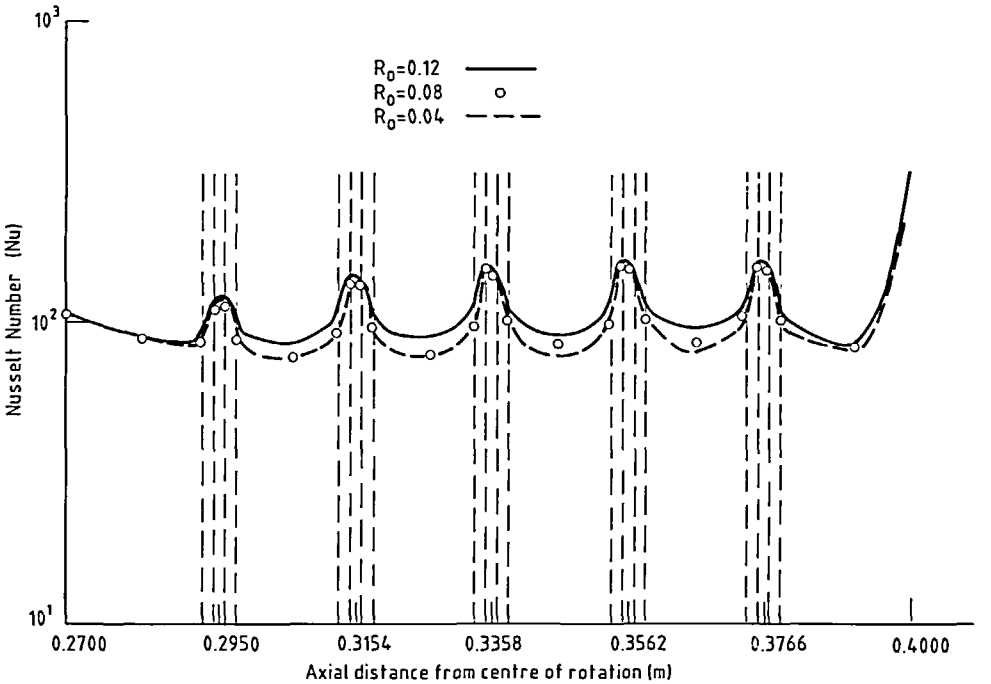

Figure 18 Predicted effects of Rossby number on the heat transfer (*Nu*) along the leading edge of a ribbed cylindrical duct (Re = 15,000)

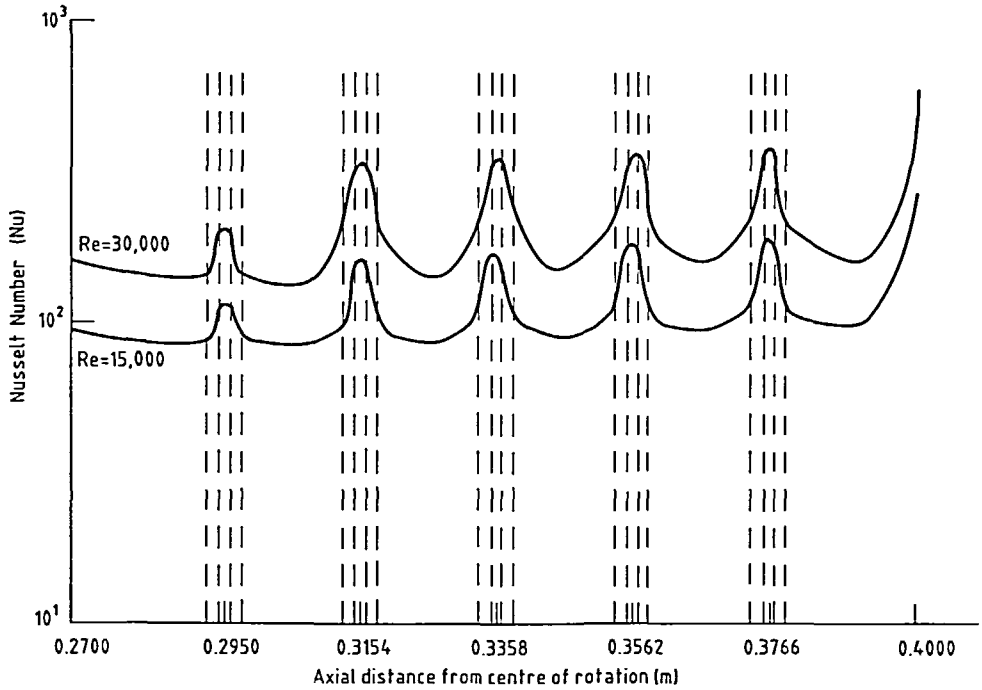

Figure 19 Predicted effects of Reynolds number on the heat transfer (*Nu*) along the inner surface of a ribbed cylindrical duct ($R_o = 0.00$)

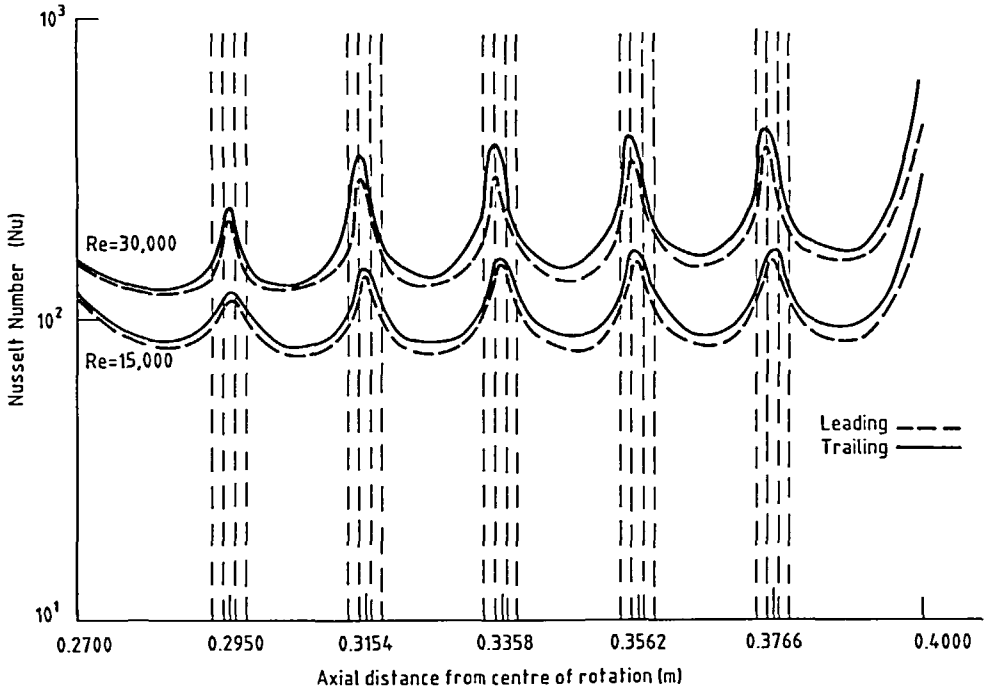

Figure 20 Predicted effects of Reynolds number on the heat transfer (*Nu*) along the inner surface of a ribbed cylindrical duct ($R_o = 0.04$)

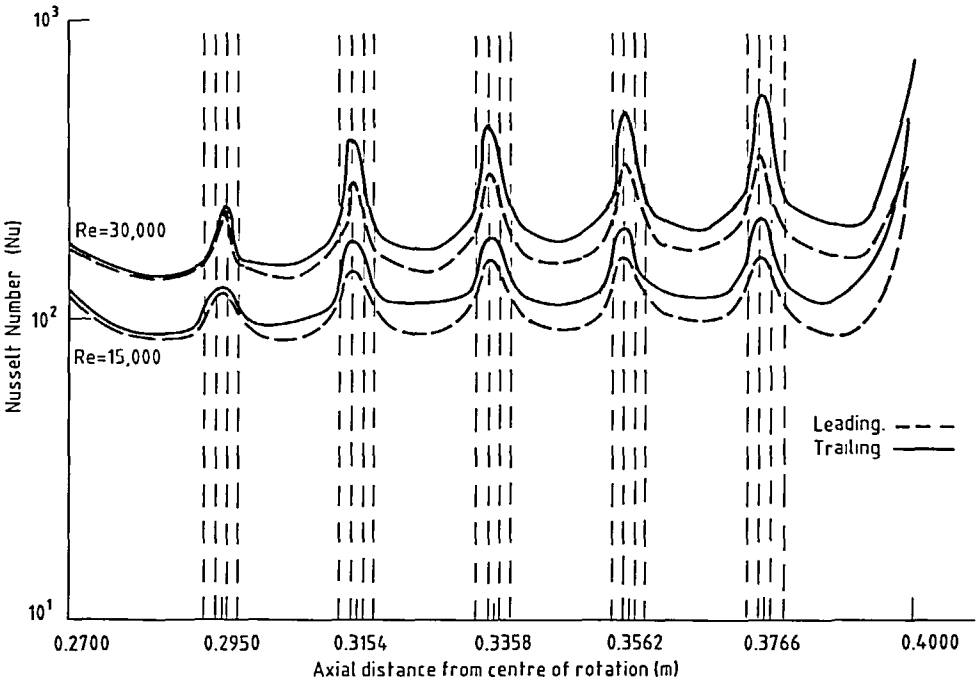

Figure 21 Predicted effects of Reynolds number on the heat transfer (*Nu*) along the inner surface of a ribbed cylindrical duct ($R_0=0.12$)

demonstrate that, as expected, a higher Reynolds number results in a higher rate of heat transfer for the same rotational speed. Again, the influence of the Coriolis force is relatively weak and limited to local variations.

CONCLUSIONS

The finite element prediction of the relative effects of the mixed geometrical and rotational mechanisms on the internal hydrodynamic and thermal patterns has been investigated. Although the Coriolis force alters the local flow patterns, the overall cooling efficiency will not exhibit a significant increase until the Rossby number exceeds a certain value. However, the inclusion of roughness of wall surface, such as ribs in this case, substantially increase heat transfer. Similar to rotating smooth ducts, the heat transfer rate is dependent on coolant inertias, although the magnitude of transfer is enhanced considerably, again, by the inclusion of the roughness.

NOMENCLATURE

C	specific heat of the fluid
$C\mu$	coefficient defined in (4)
C_D	coefficient defined in (5)
D	diameter of rotating duct
H	eccentricity of mid-plane of rotating duct
h	rib height
K	kinetic energy of turbulence
k	coefficient of thermal conductivity
L	length of rotating duct

l	length scale of turbulence
l_p	distance between each pair of ribs
P	time averaged pressure
ρ	density
Re	Reynolds number $=\rho WD/\mu$
Ro	Rossby number $=\Omega D/W$
T	time averaged temperature
U_i	time averaged velocity
μ	dynamic viscosity
μ_t	turbulent viscosity
W	mean axial velocity
X	body force
x	coordinate
σ	Prandtl number
σ_t	turbulent Prandtl number
σ_k	coefficient defined in (5)
Ω	rotational velocity
(Ω_j, x_i)	angle between Ω_j vector and x_i direction

ACKNOWLEDGEMENTS

The authors wish to acknowledge the financial support of the MOD and Rolls-Royce plc during the pursuance of this work.

REFERENCES

1 Morris, W. D. and Ayham, T. Observations on the influence of rotation on heat transfer in the coolant channels of gas turbine blades, *Proc. Inst. Mech. Eng.*, **193**, 303–311 (1979)
2 Ghavani-Nasv, G. *PhD Thesis*, University College of Swansea, Wales (1989)
3 Berg, H. P., Hennecke, D. K., Elfert, M. and Hein, O. The effect of rotation on local coolant side flow and heat transfer in turbine blades, *10th Int. Symp. Air Breathing Engines, Nottingham*, Paper No. 3.2, pp. 170–183 (1991)
4 Xia, J. Y., Taylor, C. and Medwell, J. O. Finite element modelling of the near wall zone of confined turbulent flows, *Eng. Comput.* **6**, 127–132 (1989)
5 Morris, W. D. and Salemi, R. An attempt to experimentally uncouple the effect of Coriolis and buoyancy forces on heat transfer in smooth circular tubes which rotate in the orthogonal model, *ASME Gas Turbine Aeroengine Congr., Orlando, 91-GT-17* (1991)
6 Xia, J. Y. Finite element method and complex turbulent flow and heat transfer, *PhD Thesis*, University College of Swansea, Wales (1990)
7 Taylor, C., Rance, J. and Medwell, J. O. A method for the prediction of Coriolis induced secondary flows and their influence on heat transfer in rotating ducts, *Eng. Comput.* **3**, 1–12 (1986)
8 Davies, J. T. *Turbulence Phenomena*, Academic Press, London (1972)
9 Bryant, D. Internal Memorandum, E/WJP/80085, Rolls-Royce plc., Bristol (1990)
10 Medwell, J. O., Morris, W. D., Xia, J. Y. and Taylor, C. An investigation of convective heat transfer in a rotating coolant channel, *ASME Paper 90-GT-329* (1990)
11 Taylor, C., Xia, J. Y., Medwell, J. O. and Morris, W. D. Numerical simulation of three dimensional turbulent flow and heat transfer within a multi-ribbed cyclindrical duct, *ASME Paper, 91-GT-8* (1991)